

Quantum-Ready Microwave Detection with Scalable Graphene Bolometers in the Strong Localization Regime

Yu-Cheng Chang,¹ Federico Chianese,² Naveen Shetty,² Johanna Huhtasaari,² Aditya Jayaraman,² Joonas T. Peltonen,¹ Samuel Lara-Avila,² Bayan Karimi,^{1,3} Andrey Danilov,² Jukka P. Pekola,¹ and Sergey Kubatkin^{2,4,*}

¹*Pico group, QTF Centre of Excellence, Department of Applied Physics, Aalto University, P.O. Box 15100, FI-00076 Aalto, Finland*

²*Department of Microtechnology and Nanoscience, Chalmers University of Technology, 412 96 Gothenburg, Sweden*

³*Pritzker School of Molecular Engineering, University of Chicago, Chicago IL 60637, USA*

⁴*Institute Q – the Finnish Quantum Institute, Aalto University, Finland*

(Dated: June 13, 2025)

Exploiting quantum interference of charge carriers, epitaxial graphene grown on silicon carbide emerges as a game-changing platform for ultra-sensitive bolometric sensing, featuring an intrinsic resistive thermometer response unmatched by any other graphene variant. By achieving low and uniform carrier densities, we have accessed a new regime of strong charge localization that dramatically reduces thermal conductance, significantly enhancing bolometer performance. Here we present scalable graphene-based bolometers engineered for detecting GHz-range photons, a frequency domain essential for superconducting quantum processors. Our devices deliver a state-of-the-art noise equivalent power of $40 \text{ zW}/\sqrt{\text{Hz}}$ at $T = 40 \text{ mK}$, enabled by the steep temperature dependence of thermal conductance, $G_{\text{th}} \sim T^4$ for $T < 100 \text{ mK}$. These results establish epitaxial graphene bolometers as versatile and low-back-action detectors, unlocking new possibilities for next-generation quantum processors and pioneering investigations into the thermodynamics and thermalization pathways of strongly entangled quantum systems.

Detecting extremely small powers of electromagnetic radiation is essential in modern physics, where even the faintest signals can carry valuable information. One prominent example is the search for axions—hypothetical particles that could make up dark matter—which undergo conversion into photons in a magnetic field, thus producing an extremely weak microwave radiation [1–3]. Another example is quantum information processing, where operations on qubits often involve single or few-photon signals that require precise, low-noise detection. In both cases, bolometers provide an effective solution [4–8]. These devices are temperature-dependent resistors that absorb radiation and are weakly thermally coupled to a reservoir, allowing them to register minute temperature increases. This enables accurate detection of tiny power levels without adding significant electrical noise. In a bolometer, minimizing electron-phonon coupling to the substrate is crucial to ensure that absorbed radiation effectively heats the electron system without rapidly dissipating energy to the lattice.

Graphene doped to the Dirac point is an ideal material for sensitive detection because a shrinking Fermi surface at extremely low electron density imposes phase-space restrictions for electron-phonon interactions. This allows graphene to retain absorbed energy longer, resulting in higher temperature sensitivity and improved performance for detecting extremely small power levels. However, at high carrier density graphene’s intrinsic temperature dependence of resistivity is too weak for efficient bolometer operation [9, 10]. To address this limitation, one can induce superconductivity in graphene

by coupling it to a nearby superconductor and leverage the superconducting transition. Indeed, impressive results were achieved on a Superconductor–Graphene hybrid junction, using an exfoliated graphene flake insulated by hexagonal boron nitride (hBN) [11]. Open issues that remain in this approach are scalability and, importantly, extending the operational temperature range of the proximitized-graphene bolometer, which is bound to operate close to the superconducting transition in the superconductor.

Here, we overcome these two critical shortcomings by introducing a novel platform based on epitaxial graphene grown on silicon carbide (SiC), a wafer-scale technology, allowing uniform graphene doping close to Dirac point [12]. In this system the graphene layer exhibits an intrinsic temperature dependence of resistance caused by quantum interference of carriers in the presence of strong inter-valley scattering [13–15] – a mechanism fundamentally different from superconducting proximity effects. Crucially, this response is not bound by a superconducting critical temperature; instead, device sensitivity improves continuously as temperature decreases, making it exceptionally well-suited as sensitive cryogenic radiation detector. We demonstrate that below 200 mK, quantum interference effects in graphene induce strong localization of charge carriers, pushing the graphene bolometer into a qualitatively new transport regime. This leads to a remarkable enhancement in both responsivity and thermal isolation from the reservoir, with the potential to enable unprecedented sensitivity of truly scalable graphene detectors.

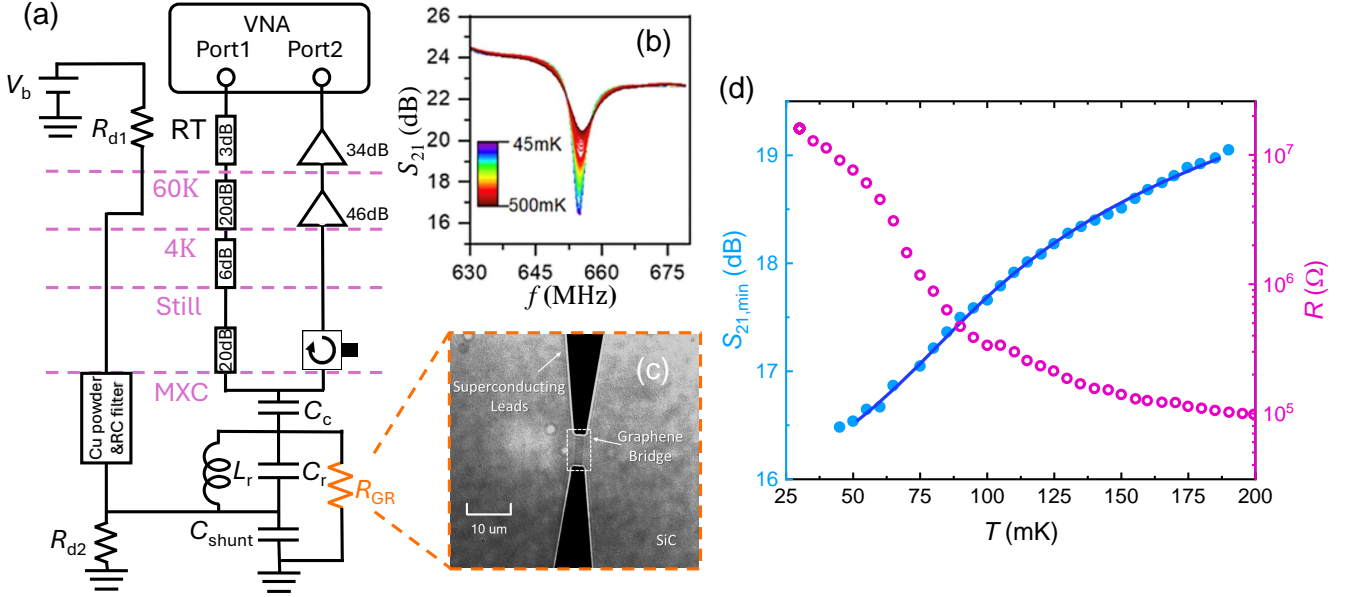


FIG. 1. Monitoring graphene electron temperature by Radio Frequency (RF). (a) Cryogenic set up for RF notched transmission measurements on graphene bridge. (b) A set of resonances on S_{21} transmission measured at different temperatures. The resonance quality factor follows the temperature dependence of graphene bridge resistance. (c) An optical transmission image of a $8 \times 2 \mu\text{m}^2$ graphene bridge, contacted by superconducting aluminum electrodes to eliminate the electronic heat transport to the leads; the $8 \mu\text{m}$ long graphene bridge suppresses undesired supercurrent due to proximity effect. (d) Transmission S_{21} for monitoring the graphene resistance and electronic temperature. The minima on transmission $S_{21}(T)$ at resonance (cf Fig. 1b) vs. the fridge temperature T (blue plot) and Direct Current (DC) resistance measurements $R(T)$ made on the same bridge (red plot). Together, $R(T)$ and $S_{21}(T)$ establish one-to-one $S_{21}(T) \leftrightarrow R$ correspondence. Both $R(T)$ and $S_{21}(T)$ have a tendency to saturate at lower temperatures – possibly due to improper thermalization (cf main text).

Importantly, the presented graphene sensor has an extremely low heat capacity approaching that of a single degree of freedom, which translates into projected energy resolution in calorimeter mode, envisioned in [16], as low as $k_B T \simeq 0.7 \text{ yJ} = 0.7 \times 10^{-24} \text{ J}$ at 50 mK. Thus it would provide a click-detector resolving a single photon with frequency above 1 GHz, which is a component of the future quantum information processing toolbox that long has been desired. Thanks to drastically different physical mechanism behind bolometric operation as compared to previous reports of graphene-based detectors, our devices perform at the state-of-the-art level, making them promising for applications in quantum information processing with superconducting qubits operating in the GHz range, and for fundamental studies in this field.

SAMPLE DESIGN AND EXPERIMENTAL SETUP

We have fabricated a wafer with 16 graphene strips with different aspect ratios, and three Hall bars, aimed to evaluate transport properties of graphene (The chip layout is in Supplementary Material, sec. S1). To thermally isolate graphene, the current leads were made of aluminum, a superconductor with T_c of about 1 K.

(See Fig. S1 in Supplementary Information.) Hall bar measurements confirmed the targeted carrier density of $n \approx 10^{10} \text{ electrons/cm}^2$, achieved by polymer-molecular doping [17]. Magneto transport data of the longitudinal resistance hinted that localization in graphene is caused by quantum interference effects, which can be eliminated by applying a modest magnetic field, breaking time-reversal symmetry (see Fig. S2 in Supplementary Information). We conclude that upon lowering electron temperature the quantum-mechanical interference of the charge carriers in graphene increases, and sets graphene into the strong localization regime, where effects of electron-electron interactions are further contributing to a steeper T -dependence of R .

In this report we will focus on the performance of two samples with higher aspect ratio, demonstrating best bolometric performance. They were 2 by 8 micrometers strips shown in Fig. 1a, measured in two different dilution refrigerators with base temperatures down to 60 and 30 mK. Above 60 mK both samples demonstrated consistent results, even though they were evaluated in different measurement set-ups. In what follows, we analyze the data taken on the sample A measured down to the lowest temperature, and present the performance of the reference sample B in the heat conductance measurements (Fig. 3a).

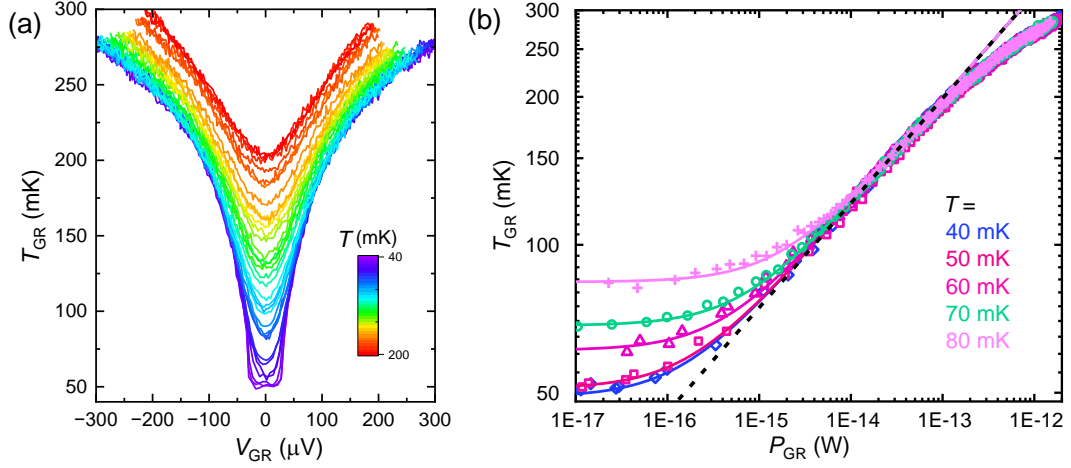


FIG. 2. (a) Graphene electronic temperature T_{GR} as a function of the DC bias voltage V_{GR} ; a set of curves taken for different cryostat temperatures. (b) Same data presented as a function of the injected DC power $V_{GR}^2/R(T_{GR})$, only the data for the lowest fridge temperatures 45 – 80 mK are presented for clarity. Symbols are for experimental data taken at cryostat temperatures 40 mK (blue rhombs), 50 mK (red squares), 60 mK (magenta triangles), 70 mK (green circles) and 80 mK (violet crosses). The solid curves are fits to a power law $T_{GR} = (P_{GR}/\sigma + T_0^\beta)^{1/\beta}$ with parameters $\beta = 4.7$, $\sigma = 2 \times 10^{-10}$ W/K $^\beta$, and $T_0 = 49.5, 51.0, 61.0, 68.5, 84.0$ mK. The straight black dashed line has a slope 4.7 ($P_{GR} \sim T_{GR}^{4.7}$).

The experimental measurement setup is schematically presented in Fig. 1; essentially we measure the heat conductance between the graphene electronic system and the substrate, using quantum interference - induced $R(T)$ as a thermometer for graphene electronic system, assuming that the substrate temperature follows the base temperature of the cryostat. To monitor graphene resistance with good precision and minimal heat load we used an RF scheme, suggested in [18]: relatively high graphene resistance was matched to the input resistance of a low noise amplifier at a frequency of 650 MHz by a lumped-element resonator with a quality factor $Q \approx 100$. A separate DC line allowed us to apply a control power to the graphene sample (See Fig. 1a). The RF scheme was accompanied by a DC measurement setup, which was also used for the bolometer calibration with heating at a known Joule power, while monitoring the electronic temperature of graphene by the RF conductance measurements. To avoid sample overheating by the RF probe power, we performed measurements at low RF powers – the detailed information will be presented in the discussion section and Supporting Information. The DC bias line was filtered/thermalized by the termocoax, followed by lumped element filters - its thermalization was checked in separate experiments.

Figure 1d presents the calibration data for RF read out of the graphene electronic temperature: both graphene resistance R and transmission resonance $S_{21,min}$ were measured as a function of the fridge temperature T . Cooperatively, $R(T)$ and $S_{21,min}(T)$ define the minimum on transmission $S_{21,min}$ as a function of graphene resistance $S_{21,min}(R)$ (technically, both $R(T)$ and $S_{21,min}(T)$ were interpolated with polynoms - cf Supplementary Sec. 3,4

- to compose the $S_{21,min}(T)$ functional dependence).

BOLOMETRIC RESPONSE OF GRAPHENE SENSOR

Having the thermometry set up calibrated (Fig. 1d), we applied a DC voltage to graphene terminals, overheating the strip, and measured the graphene electronic temperature in response to DC heating. The result is shown in Fig. 2a, where we present graphene electronic temperature T_{GR} as a function of the DC bias voltage; the cryostat temperature T being the parameter. Note that as the bridge resistance diverges at $T \rightarrow 0$, for any given bias voltage V the injected power $V^2/R \rightarrow 0$, so that below some temperature the power dissipated on graphene becomes lower than uncontrolled heat flux from non-thermalized environment (see sec. Discussion and Outlook for details). This is why the $T_{GR}(V_{GR})$ curves taken at the lowest temperatures (≤ 50 mK) are flattened around the minima.

As the next step, we can map the voltages on the horizontal axis onto dissipated powers: for any point (V_{GR}, T_{GR}) in Fig. 2a the calibration curve in Fig. 1d (blue) gives us the graphene temperature, and the corresponding dissipated power is thus $V_{GR}^2/R(T_{GR})$. The result of this transformation is presented in Fig. 2b, only the plots for the lowest fridge temperatures are shown. Figure 2b is the central plot of this contribution which presents the bolometric response of the graphene device. Together with experimental data, the Fig. 2b also presents fits to standard bolometric equation $P_{GR} = \sigma(T_{GR}^\beta - T_0^\beta)$ [19], which is based on the

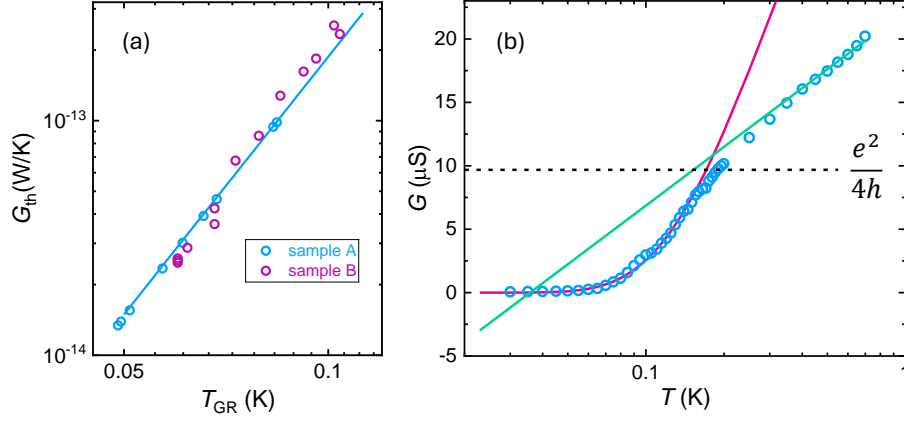


FIG. 3. (a) Graphene thermal conductance $G_{\text{th}}(T_{\text{GR}}) = \beta\sigma T_{\text{GR}}^{(\beta-1)}$ as a function of graphene temperature T_{GR} , presented are the data for two samples with of identical dimensions $W \times L = 2 \times 8 \mu\text{m}^2$, measured in two different cryostats (with base temperatures 30 mK for sample A and 60 mK for sample B). Both data sets have similar slope $\beta - 1 \approx 3.7$ in log-log plot. The blue solid line is for fit $G_{\text{th}}(T_{\text{GR}}) = 5\sigma T_{\text{GR}}^{3.7}$ with $\sigma = 2 \times 10^{-10} \text{ W/K}^{3.7}$. (b) Graphene conductance as a function of temperature. Red curve is a fit to Arrhenius law $\ln(G_{\text{GR}}) = -E_{\text{Arr}}/(k_B T_{\text{GR}}) - 9.67$ with $E_{\text{Arr}} = k_B \times 0.32 \text{ K}$. Green line presents logarithmic dependence $\frac{G_{\square}}{4} \frac{e^2}{h} \ln(\frac{T}{T'})$ with $G_{\square} = 0.69$ and $T' = 0.0358 \text{ K}$. Transition from weak to strong localisation occurs at per square conductivity of the order of e^2/h (dashed black line), consistent with interference-induced Anderson localization picture [15].

power balance condition between the graphene strip and its environment. If the environment is perfectly thermalized, T_0 matches the fridge temperature T , but it is not uncommon that below 100 mK the effective environment temperature does not follow T , see more in the section ‘Discussion and Outlook’. For all fridge temperatures presented in Fig. 2b the fit, optimized for intermediate power range (10^{-15} – 10^{-13}) W, returns the same values for parameters $\sigma = 2 \times 10^{-10} \text{ W/K}^{\beta}$ and $\beta = 4.7$; at higher temperatures the exponent slowly raises up to $\beta = 4.8$ at 200 mK (more arguments in favour of $\beta \approx 5$ are presented in Supplementary sec. S5). We note that at zero power the plots taken at 60 mK and above saturate to the fridge temperature, consistent with graphene being perfectly thermalized to the substrate. However, at the lower temperatures, the graphene temperature saturates to 50 mK regardless of the fridge temperature (for a full data set taken at different fridge temperatures consult the Supplementary sec. S6).

At high powers/temperatures we observe a deviation from $T^{4.7}$ power dependence, apparently linked to the leakage of heat through quasiparticles in Al superconducting leads [20].

ELECTRON-PHONON COUPLING AND NOISE EQUIVALENT POWER

Having the numbers for σ , β , and T_0 in $P_{\text{GR}} = \sigma(T_{\text{GR}}^{\beta} - T_0^{\beta})$, we can compose a plot for thermal conductance $G_{\text{th}}(T_{\text{GR}}) = dP_{\text{GR}}/dT_{\text{GR}} = \beta\sigma T_{\text{GR}}^{(\beta-1)}$, presented in Fig. 3a. The data for two graphene strips with the same geometry, $2 \times 8 \mu\text{m}^2$ have been evaluated in

two different cryostats; although the lowest temperature was different in the two setups, we see that the thermal conductivity G_{th} in both experiments follows a universal power law $G_{\text{th}} \sim T^{3.7}$ (blue line in Fig. 3a). The power law $G_{\text{th}} \sim T^{3.7}$ is consistent with the encouraging observation $P \sim T^{4.7}$, shown in Fig. 2b. It has much stronger temperature dependence than previously reported electron-phonon couplings in graphene [10, 21–26].

This observation correlates with another unexpected result, which is the observation of Arrhenius type conductivity for $T < 200 \text{ mK}$ (Fig. 3b). Altogether, they suggest that we reach new physics in the heat transfer process from the graphene electronic system to the substrate lattice. We attribute this novel heat transfer regime to the onset of strong localization of charge carriers at low temperatures, caused by quantum interference of the charge carriers in graphene in the presence of a specific type of disorder - such a scenario was mentioned in [27, 28].

The unusual electron-phonon decoupling observed in this experiment carries profound implications for the performance of graphene as a bolometer. The figure of merit for a bolometer is its Noise Equivalent Power (NEP) [29, 30], obtained from the standard formula $\text{NEP} = \sqrt{4k_B T_{\text{GR}}^2 G_{\text{th}}} \sim T_{\text{GR}}^{2.85}$. We see that the measured electron-phonon coupling allows for the estimate of NEP of about $40 \text{ zW}/\sqrt{\text{Hz}}$ at $T = 40 \text{ mK}$, still limited by thermalization issues. The projected NEP for properly thermalized graphene at 40 mK would thus surpass the best so far reported number $20 \text{ zW}/\sqrt{\text{Hz}}$ [31].

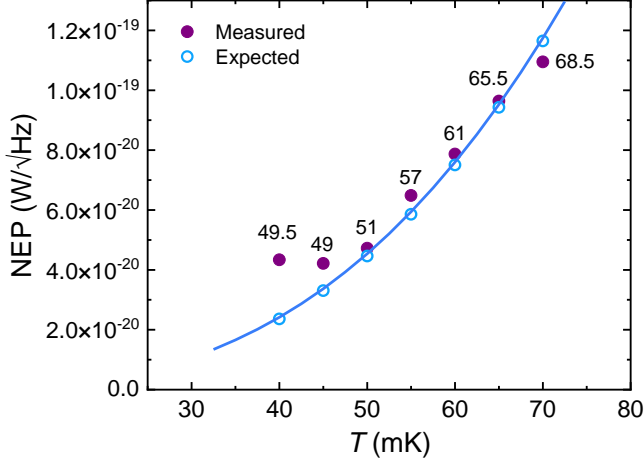


FIG. 4. Noise Equivalent Power (NEP) of graphene bolometer as found experimentally (violet circles; the numbers next to markers are for the graphene electronic temperatures T_0 - cf Fig. 2) and as expected for the case of graphene sample thermalized to a fridge temperature (blue circles). The blue line corresponds to $\sqrt{4k_B T^2 G_{th}}$ with parameters $\beta = 4.7$ and $\sigma = 2 \times 10^{-10} \text{ W/K}^{4.7}$.

DISCUSSION AND OUTLOOK

We have measured electronic temperature of our graphene device with RF transmission technique as a function of applied DC power to graphene and estimated G_{th} from these data. Applying a standard approach for the graphene bolometer performance evaluation in terms of $NEP = \sqrt{4k_B T^2 G_{th}}$, we evaluate our graphene bolometer performance as $\sim 40 \text{ zW}/\sqrt{\text{Hz}}$ evaluated at 40 mK cryostat base temperature. The observed saturation of graphene temperature at low T cannot be explained by microwave heating or measurement artifacts. Even under conservative estimates, the power dissipated in graphene from the applied microwave excitation is approximately 14 aW, corresponding to a negligible temperature increase of about 4.5 mK, which is insufficient to account for the observed saturation. A detailed analysis of this power estimation is provided in SI section 8. The saturation is therefore more likely due to the heat load from non-thermalized components of the environment such as two-level fluctuators in the substrate dielectric and/or non-equilibrium quasiparticles in aluminum leads. It is a common knowledge that the heat exchange with non-thermalized environment leads to temperature saturation in engineered quantum devices at the level of 50–70 mK [32–41], consistent with our observations. Under proper thermalization conditions, the projected NEP for 10 mK is $0.35 \text{ zW}/\sqrt{\text{Hz}}$; that is not far from the estimate made in our previous work [24]. The main difference between the work [24] and the current measurement is in the lower temperature range, providing an opportunity to convincingly reach the strong localization

regime, favoring better bolometric performance at low temperatures. We attribute this result to a synergetic effect of the onset of strong localization of charge carriers in graphene at low temperatures, caused by quantum interference of charge carriers and a consequence of a better, lower noise, less invasive, graphene temperature readout, provided by the RF transmission scheme, implemented in this work. To get a better bolometric performance we need to improve graphene thermalization at low temperatures, which for a bolometric device is especially challenging due to the otherwise beneficial, or even mandatory, thermal decoupling of the graphene bridge from the phonon bath.

In view of prospective calorimetric applications [42], it is instructive to evaluate the heat capacity of the graphene bridge. The Fermi energy in graphene is $E_F = \hbar v_F \sqrt{\pi n}$ [43, 44], for Fermi velocity $v_F = 1 \times 10^6 \text{ m/s}$ and for the carrier density $n = 10^{10} \text{ cm}^{-2}$ we arrive at $E_F/k_B = 122 \text{ K}$. Assuming operation temperature $T = 50 \text{ mK}$, we can estimate the number of electrons in a $k_B T$ slice around E_F (the one contributing to the heat capacity) for $S = 2 \times 8 \text{ } \mu\text{m}^2$ graphene bridge as $2 \frac{k_B T}{E_F} n S \sim 1$. This is quite a remarkable result which shows that as a bolometric sensor, our graphene bridge is equivalent to a quantum dot with a single degree of freedom and the heat capacity $C_e \sim k_B$. The energy resolution is then [45, 46] $\Delta E = \sqrt{k_B T^2 C_e} \sim k_B T = 0.7 \times 10^{-24} \text{ J} = 0.7 \text{ yJ}$, which corresponds to an energy of a single 1 GHz photon.

CONCLUSIONS

To conclude, we demonstrated that a simple and scalable graphene micrometer-sized strip, cooled to millikelvin temperatures, offers zeptoWatt sensitivity in a bolometric regime, thanks to its temperature-dependent resistance, caused by quantum interference effects, and thermal decoupling. This performance opens the path for scalable high-performance devices in quantum information technology such as click-detector resolving a single 1 GHz photon, or for effective realization of solid-state multi-channel quantum tomography [47]. Moreover, our technology could be suitable to tackle challenges in cosmology and astronomy, fields where traditional detection of faint radiation has resulted in major breakthroughs [48]. Finally, the device core graphene bridge, hosting interacting 2D electrons in strongly localized regime, is a promising object for studies of thermalization dynamics of non-ergodic many body localized systems [49].

ACKNOWLEDGEMENTS

This work at Chalmers was jointly supported by the Chalmers Area of Advance Nano, Chalmers Area of

Advanced materials, 2D TECH VINNOVA competence Center (Ref. 2019-00068), Swedish Research Council VR (Contract Nos. 2021-05252), and Knut and Alice Wallenberg foundation via the Wallenberg Center for Quantum Technology (WACQT); A.D. acknowledges support from the Horizon Europe EIC Pathfinder project 101115190 IQARO. Sample fabrication and analysis was supported by Myfab Chalmers and Chalmers Materials Analysis Laboratory (CMAL). This work at Aalto was supported by the Research Council of Finland Centre of Excellence programme grant 336810 and grant 349601 (THEPOW). We sincerely acknowledge the facilities and technical support of Otaniemi Research Infrastructure for Micro and Nanotechnologies (OtaNano) to perform this research. B. K. acknowledges the European Union's Research and Innovation Programme, Horizon Europe, under the Marie Skłodowska-Curie Grant Agreement No. 101150440 (Tc-QTD). We are grateful for discussions with Floriana Lombardi, Dmitry S. Golubev, Igor V. Lerner, and Tord Claeson.

* sergey.kubatkin@chalmers.se

- [1] C. M. Adair, K. Altenmüller, V. Anastassopoulos, S. Arguedas Cuendis, J. Baier, K. Barth, A. Belov, D. Bozicevic, H. Bräuninger, G. Cantatore, F. Caspers, J. F. Castel, S. A. Çetin, W. Chung, H. Choi, J. Choi, T. Dafni, M. Davenport, A. Dermenev, K. Desch, B. Döbrich, H. Fischer, W. Funk, J. Galan, A. Gardikiotis, S. Gninenko, J. Golm, M. D. Hasinoff, D. H. H. Hoffmann, D. Díez Ibáñez, I. G. Irastorza, K. Jakovčić, J. Kaminski, M. Karuza, C. Krieger, c. Kutlu, B. Lakić, J. M. Laurent, J. Lee, S. Lee, G. Luzón, C. Malbrunot, C. Margalejo, M. Maroudas, L. Miceli, H. Mirallas, L. Obis, A. Özbey, K. Özbozduman, M. J. Pivovarov, M. Rosu, J. Ruz, E. Ruiz-Chóliz, S. Schmidt, M. Schumann, Y. K. Semertzidis, S. K. Solanki, L. Stewart, I. Tsagris, T. Vafeiadis, J. K. Vogel, M. Vretenar, S. Youn, and K. Zioutas, Search for Dark Matter Axions with CAST-CAPP, *Nat. Commun.* **13**, 6180 (2022).
- [2] T. Braine, R. Cervantes, N. Crisosto, N. Du, S. Kimes, L. J. Rosenberg, G. Rybka, J. Yang, D. Bowring, A. S. Chou, R. Khatiwada, A. Sonnenschein, W. Wester, G. Carosi, N. Woollett, L. D. Duffy, R. Bradley, C. Boutan, M. Jones, B. H. LaRoque, N. S. Oblath, M. S. Taubman, J. Clarke, A. Dove, A. Eddins, S. R. O'Kelley, S. Nawaz, I. Siddiqi, N. Stevenson, A. Agrawal, A. V. Dixit, J. R. Gleason, S. Jois, P. Sikivie, J. A. Solomon, N. S. Sullivan, D. B. Tanner, E. Lentz, E. J. Daw, J. H. Buckley, P. M. Harrington, E. A. Henriksen, K. W. Murch, and ADMX Collaboration, Extended Search for the Invisible Axion with the Axion Dark Matter Experiment, *Phys. Rev. Lett.* **124**, 101303 (2020).
- [3] A. L. Pankratov, A. V. Gordeeva, A. V. Chiginev, L. S. Revin, A. V. Blagodatkin, N. Crescini, and L. S. Kuzmin, Detection of single-mode thermal microwave photons using an underdamped Josephson junction, *Nat. Commun.* **16**, 3457 (2025).
- [4] I. G. Irastorza and J. Redondo, New experimental approaches in the search for axion-like particles, *Prog. Part. Nucl. Phys.* **102**, 89 (2018).
- [5] P. Sikivie, Experimental Tests of the "Invisible" Axion, *Phys. Rev. Lett.* **51**, 1415 (1983).
- [6] T. M. Shokair, J. Root, K. A. Van Bibber, B. Brubaker, Y. V. Gurevich, S. B. Cahn, S. K. Lamoreaux, M. A. Anil, K. W. Lehnert, B. K. Mitchell, A. Reed, and G. Carosi, Future directions in the microwave cavity search for dark matter axions, *Int. J. Mod. Phys. A* **29**, 1443004 (2014).
- [7] B. Karimi and J. P. Pekola, Quantum Trajectory Analysis of Single Microwave Photon Detection by Nanocalorimetry, *Phys. Rev. Lett.* **124**, 170601 (2020).
- [8] A. M. Gunyhó, S. Kundu, J. Ma, W. Liu, S. Niemelä, G. Catto, V. Vadimov, V. Vesterinen, P. Singh, Q. Chen, and M. Möttönen, Single-shot readout of a superconducting qubit using a thermal detector, *Nat. Electron.* **7**, 288 (2024).
- [9] C. B. McKittrick, D. E. Prober, H. Vora, and X. Du, Ultrasensitive graphene far-infrared power detectors, *J. Phys.: Condens. Matter* **27**, 164203 (2015).
- [10] D. K. Efetov and P. Kim, Controlling Electron-Phonon Interactions in Graphene at Ultrahigh Carrier Densities, *Phys. Rev. Lett.* **105**, 256805 (2010).
- [11] R. Kokkonen, J.-P. Girard, D. Hazra, A. Laitinen, J. Govenius, R. E. Lake, I. Sallinen, V. Vesterinen, M. Partanen, J. Y. Tan, K. W. Chan, K. Y. Tan, P. Hakonen, and M. Möttönen, Bolometer operating at the threshold for circuit quantum electrodynamics, *Nature* **586**, 47 (2020).
- [12] H. He, K. Cedergren, N. Shetty, S. Lara-Avila, S. Kubatkin, T. Bergsten, and G. Eklund, Accurate graphene quantum Hall arrays for the new International System of Units, *Nat. Commun.* **13**, 6933 (2022).
- [13] E. McCann, K. Kechedzhi, V. I. Fal'ko, H. Suzuura, T. Ando, and B. L. Altshuler, Weak-Localization Magnetoresistance and Valley Symmetry in Graphene, *Phys. Rev. Lett.* **97**, 146805 (2006).
- [14] S. Lara-Avila, A. Tzalenchuk, S. Kubatkin, R. Yakimova, T. J. B. M. Janssen, K. Cedergren, T. Bergsten, and V. Fal'ko, Disordered Fermi Liquid in Epitaxial Graphene from Quantum Transport Measurements, *Phys. Rev. Lett.* **107**, 166602 (2011).
- [15] L. A. Ponomarenko, A. K. Geim, A. A. Zhukov, R. Jalil, S. V. Morozov, K. S. Novoselov, I. V. Grigorieva, E. H. Hill, V. V. Cheianov, V. I. Fal'ko, K. Watanabe, T. Taniguchi, and a. R. V. Gorbachev, Tunable metal-insulator transition in double-layer graphene heterostructures, *Nat. Phys.* **7**, 958 (2011).
- [16] M. L. Roukes, Yoctocalorimetry: phonon counting in nanostructures, *Physica B: Condensed Matter* **263-264**, 1 (1999).
- [17] H. He, K. H. Kim, A. Danilov, D. Montemurro, L. Yu, Y. W. Park, F. Lombardi, T. Bauch, K. Moth-Poulsen, T. Iakimov, R. Yakimova, P. Malmberg, C. Müller, S. Kubatkin, and S. Lara-Avila, Uniform doping of graphene close to the Dirac point by polymer-assisted assembly of molecular dopants, *Nat. Commun.* **9**, 3956 (2018).
- [18] R. J. Schoelkopf, P. Wahlgren, A. A. Kozhevnikov, P. Delsing, and D. E. Prober, The Radio-Frequency Single-Electron Transistor (RF-SET): A Fast and Ultrasensitive Electrometer, *Science* **280**, 1238 (1998).

- [19] V. F. Gantmakher, The experimental study of electron-phonon scattering in metals, *Rep. Prog. Phys.* **37**, 317 (1974).
- [20] K. L. Viisanen and J. P. Pekola, Anomalous electronic heat capacity of copper nanowires at sub-Kelvin temperatures, *Phys. Rev. B* **97**, 115422 (2018).
- [21] A. C. Betz, F. Vialla, D. Brunel, C. Voisin, M. Picher, A. Cavanna, A. Madouri, G. Fève, J.-M. Berroir, B. Plaças, and E. Pallecchi, Hot Electron Cooling by Acoustic Phonons in Graphene, *Phys. Rev. Lett.* **109**, 056805 (2012).
- [22] I. V. Borzenets, U. C. Coskun, H. T. Mebrahtu, Y. V. Bomze, A. I. Smirnov, and G. Finkelstein, Phonon Bottleneck in Graphene-Based Josephson Junctions at Millikelvin Temperatures, *Phys. Rev. Lett.* **111**, 027001 (2013).
- [23] S. Lara-Avila, A. Danilov, D. Golubev, H. He, K. H. Kim, R. Yakimova, F. Lombardi, T. Bauch, S. Cherednichenko, and S. Kubatkin, Towards quantum-limited coherent detection of terahertz waves in charge-neutral graphene, *Nat. Astron.* **3**, 983 (2019).
- [24] B. Karimi, H. He, Y. C. Chang, L. Wang, J. P. Pekola, R. Yakimova, N. Shetty, J. T. Peltonen, S. Lara-Avila, and S. Kubatkin, Electron-phonon coupling of epigraphene at millikelvin temperatures measured by quantum transport thermometry, *Appl. Phys. Lett.* **118**, 103102 (2021).
- [25] A. El Fatimy, R. L. Myers-Ward, A. K. Boyd, K. M. Daniels, D. K. Gaskill, and P. Barbara, Epitaxial graphene quantum dots for high-performance terahertz bolometers, *Nat. Nanotechnol.* **11**, 335 (2016).
- [26] A. El Fatimy, P. Han, N. Quirk, L. St. Marie, M. T. Dejarld, R. L. Myers-Ward, K. Daniels, S. Pavunny, D. K. Gaskill, Y. Aytac, T. E. Murphy, and P. Barbara, Effect of defect-induced cooling on graphene hot-electron bolometers, *Carbon* **154**, 497 (2019).
- [27] G. McArdle and I. V. Lerner, Electron-phonon decoupling in two dimensions, *Sci. Rep.* **11**, 24293 (2021).
- [28] W. Chen and A. A. Clerk, Electron-phonon mediated heat flow in disordered graphene, *Phys. Rev. B* **86**, 125443 (2012).
- [29] F. J. Low, Low-Temperature Germanium Bolometer, *J. Opt. Soc. Am.* **51**, 1300 (1961).
- [30] P. L. Richards, Bolometers for infrared and millimeter waves, *Journal of Applied Physics* **76**, 1 (1994).
- [31] R. Kokkonen, J. Govenius, V. Vesterinen, R. E. Lake, A. M. Gunyhó, K. Y. Tan, S. Simbierowicz, L. Grönberg, J. Lehtinen, M. Prunnila, J. Hassel, A. Lamminen, O.-P. Saira, and M. Möttönen, Nanobolometer with ultralow noise equivalent power, *Commun. Phys.* **2**, 1 (2019).
- [32] X. Y. Jin, A. Kamal, A. P. Sears, T. Gudmundsen, D. Hover, J. Miloshi, R. Slattery, F. Yan, J. Yoder, T. P. Orlando, S. Gustavsson, and W. D. Oliver, Thermal and Residual Excited-State Population in a 3D Transmon Qubit, *Phys. Rev. Lett.* **114**, 240501 (2015).
- [33] A. Kulikov, R. Navarathna, and A. Fedorov, Measuring Effective Temperatures of Qubits Using Correlations, *Phys. Rev. Lett.* **124**, 240501 (2020).
- [34] A. Sultanov, M. Kuzmanović, A. V. Lebedev, and G. S. Paraoanu, Protocol for temperature sensing using a three-level transmon circuit, *Applied Physics Letters* **119**, 144002 (2021).
- [35] D. S. Lvov, S. A. Lemziakov, E. Ankerhold, J. T. Peltonen, and J. P. Pekola, Thermometry based on a superconducting qubit, *Phys. Rev. Appl.* **23**, 054079 (2025).
- [36] H. Paik, D. I. Schuster, L. S. Bishop, G. Kirchmair, G. Catelani, A. P. Sears, B. R. Johnson, M. J. Reagor, L. Frunzio, L. I. Glazman, S. M. Girvin, M. H. Devoret, and R. J. Schoelkopf, Observation of High Coherence in Josephson Junction Qubits Measured in a Three-Dimensional Circuit QED Architecture, *Phys. Rev. Lett.* **107**, 240501 (2011).
- [37] J. Burnett, L. Faoro, I. Wisby, V. L. Gurtovoi, A. V. Chernykh, G. M. Mikhailov, V. A. Tulin, R. Shaikhaidarov, V. Antonov, P. J. Meeson, A. Y. Tzalenchuk, and T. Lindström, Evidence for interacting two-level systems from the $1/f$ noise of a superconducting resonator, *Nat. Commun.* **5**, 4119 (2014).
- [38] S. E. de Graaf, L. Faoro, J. Burnett, A. A. Adamyan, A. Y. Tzalenchuk, S. E. Kubatkin, T. Lindström, and A. V. Danilov, Suppression of low-frequency charge noise in superconducting resonators by surface spin desorption, *Nat. Commun.* **9**, 1143 (2018).
- [39] M. Lucas, A. V. Danilov, L. V. Levitin, A. Jayaraman, A. J. Casey, L. Faoro, A. Y. Tzalenchuk, S. E. Kubatkin, J. Saunders, and S. E. de Graaf, Quantum bath suppression in a superconducting circuit by immersion cooling, *Nat. Commun.* **14**, 3522 (2023).
- [40] S. E. de Graaf, A. A. Adamyan, T. Lindström, D. Erts, S. E. Kubatkin, A. Y. Tzalenchuk, and A. V. Danilov, Direct Identification of Dilute Surface Spins on Al₂O₃: Origin of Flux Noise in Quantum Circuits, *Phys. Rev. Lett.* **118**, 057703 (2017).
- [41] C. M. Quintana, Y. Chen, D. Sank, A. G. Petukhov, T. C. White, D. Kafri, B. Chiaro, A. Megrant, R. Barends, B. Campbell, Z. Chen, A. Dunsworth, A. G. Fowler, R. Graff, E. Jeffrey, J. Kelly, E. Lucero, J. Y. Mutus, M. Neeley, C. Neill, P. J. J. O'Malley, P. Roushan, A. Shabani, V. N. Smelyanskiy, A. Vainsencher, J. Wenner, H. Neven, and J. M. Martinis, Observation of Classical-Quantum Crossover of $1/f$ Flux Noise and Its Paramagnetic Temperature Dependence, *Phys. Rev. Lett.* **118**, 057702 (2017).
- [42] C. D. Satrya, Y.-C. Chang, A. S. Strelnikov, R. Upadhyay, I. K. Mäkinen, J. T. Peltonen, B. Karimi, and J. P. Pekola, Thermal spectrometer for superconducting circuits, *Nat. Commun.* **16**, 4435 (2025).
- [43] A. H. Castro Neto, F. Guinea, N. M. R. Peres, K. S. Novoselov, and A. K. Geim, The electronic properties of graphene, *Rev. Mod. Phys.* **81**, 109 (2009).
- [44] S. Das Sarma, S. Adam, E. H. Hwang, and E. Rossi, Electronic transport in two-dimensional graphene, *Rev. Mod. Phys.* **83**, 407 (2011).
- [45] S. H. Moseley, J. C. Mather, and D. McCammon, Thermal detectors as x-ray spectrometers, *Journal of Applied Physics* **56**, 1257 (1984).
- [46] G.-H. Lee, D. K. Efetov, W. Jung, L. Ranzani, E. D. Walsh, T. A. Ohki, T. Taniguchi, K. Watanabe, P. Kim, D. Englund, and K. C. Fong, Graphene-based Josephson junction microwave bolometer, *Nature* **586**, 42 (2020).
- [47] L. Pereira, J. J. Garcia-Ripoll, and T. Ramos, Parallel tomography of quantum non-demolition measurements in multi-qubit devices, *npj Quantum Inf* **9**, 1 (2023).
- [48] F. Paolucci, N. Ligato, G. Germanese, V. Buccheri, and F. Giazotto, Fully Superconducting Josephson Bolometers for Gigahertz Astronomy, *Applied Sciences* **11**, 746 (2021).

- [49] M. Ueda, Quantum equilibration, thermalization and prethermalization in ultracold atoms, *Nat. Rev. Phys.* **2**, 669 (2020).

SUPPLEMENTARY INFORMATION

Quantum-Ready Microwave Detection with Scalable Graphene Bolometers in the Strong Localization Regime

Yu-Cheng Chang¹, Federico Chianese², Naveen Shetty², Johanna Huhtasaari², Aditya Jayaraman², Joonas T. Peltonen¹, Samuel Lara-Avila², Bayan Karimi^{1,3}, Andrey Danilov², Jukka P. Pekola¹, Sergey Kubatkin²

¹*Pico group, QTF Centre of Excellence, Department of Applied Physics, Aalto University, P.O. Box 15100, FI-00076 Aalto, Finland*

²*Department of Microtechnology and Nanoscience, Chalmers University of Technology, 412 96 Gothenburg, Sweden*

³*Pritzker School of Molecular Engineering, University of Chicago, Chicago IL 60637, USA*

S1. Chip layout

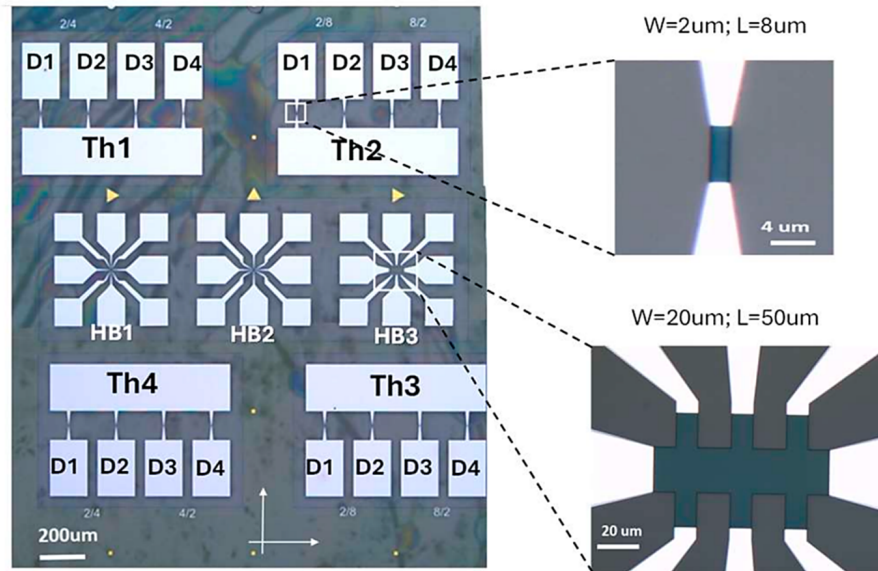


Fig. S1. Chip layout: reflection image in the optical microscope; one of the graphene stripes $2 \times 8 \mu^2$ is presented, together with the Hall bar HB3, examined for magnetotransport. Bright leads represent Al film.

S2. Magnetotransport measurements on the Hall bar HB3, taken in the dilution fridge.

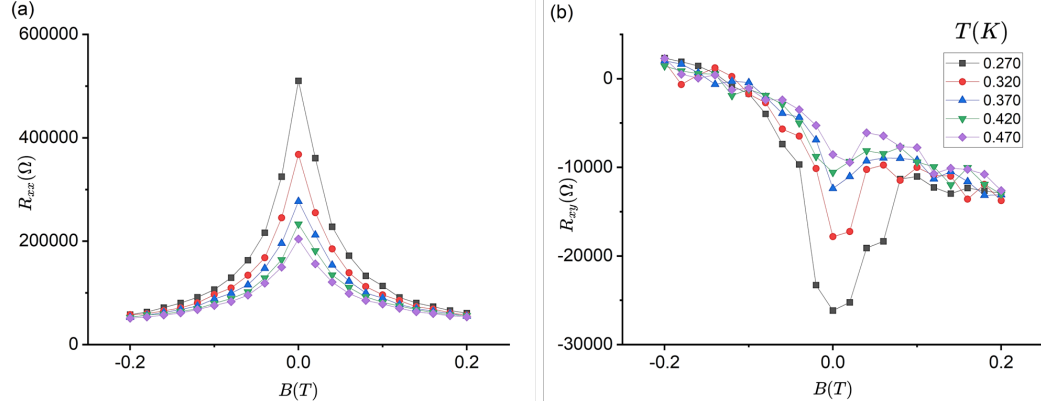


Fig. S2. Magnetotransport measurements on graphene Hall bar HB3, taken at several temperatures: 270, 320, 370, 420, and 470 mK. (a) R_{xx}/\square (b) plot, demonstrating delocalization of graphene charge carriers in magnetic field, breaking time-reversal symmetry. (b) R_{xy} measured on the same Hall bar: an obvious mixing of R_{xy} and R_{xx} at zero field is present, but an overall slope 25 kΩ/T can be seen, which is consistent with the estimate of the carrier density of $1.5 \cdot 10^{10} \text{ cm}^{-2}$.

S3. $S_{21}(T)$ calibration plot.

Transmission S_{21} at $V_{\text{base}}=0$ was measured separately with a longer averaging time at fridge temperatures in the range 40-200 mK to compose $S_{21} \rightarrow T_{\text{GR}}$ calibration plot:

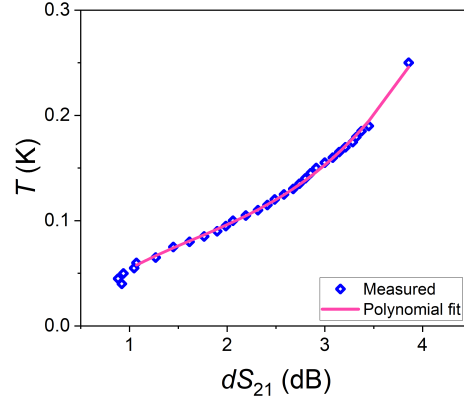


Fig. S3. $S_{21} \rightarrow T_{\text{GR}}$ calibration plot. The calibration curve is the best polynomial fit $T_{\text{GR}}(S_{21}) = a \cdot (dS_{21})^3 + b \cdot (dS_{21})^2 + c \cdot (dS_{21}) + d$, where $dS_{21} = S_{21} - 15.6$ dB, $a = 0.00715$, $b = -0.03543$, $c = 0.09803$, and $d = -0.01529$. The polynomial fit was done for temperatures in the range 60 mK – 200 mK to exclude the area where sample temperature saturates.

S4. $R(T)$ calibration plot.

The graphene resistance was measured at dc as a function of fridge temperature (at zero bias voltage).

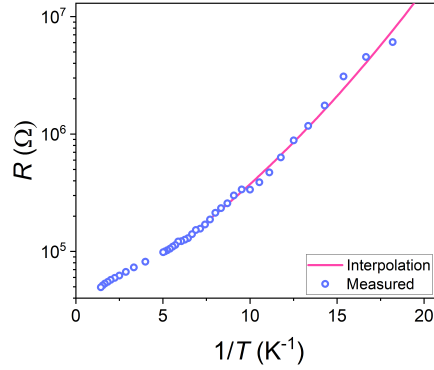


Fig. S4. Graphene resistance R versus temperature T . The interpolation curve is given by $\ln(R) = \frac{a}{T^2} + \frac{b}{T} + c$, where $a = 0.00701$, $b = 0.1703$, $c = 10.43$

S5. Graphene temperature vs. heating power: $P_{GR} \sim T_{GR}^5$ vs. $P_{GR} \sim T_{GR}^4$.

To evaluate the exponent β in $P_{GR} \sim T_{GR}^\beta$ we composed two plots: T_{GR}^5 and T_{GR}^4 versus dissipated power P_{GR} :

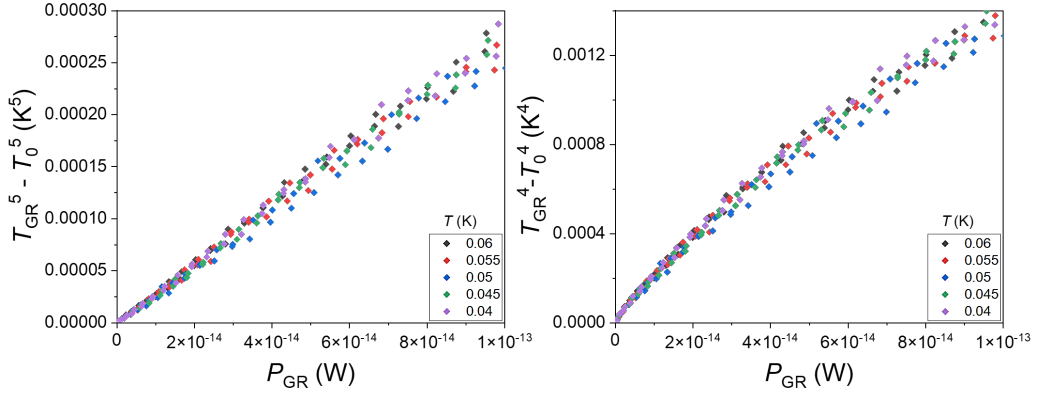


Fig. S5. Graphene temperature in the T_{GR} in the fifth (left) and fourth (right) power versus the power P_{GR} dissipated in graphene. Note the straight linear dependence in the left plot.

We see that in $T_{GR}^5(P_{GR})$ all data points aggregate along the straight line, suggesting that β is close to 5.

S6. Graphene temperature vs. heating power: full data set.

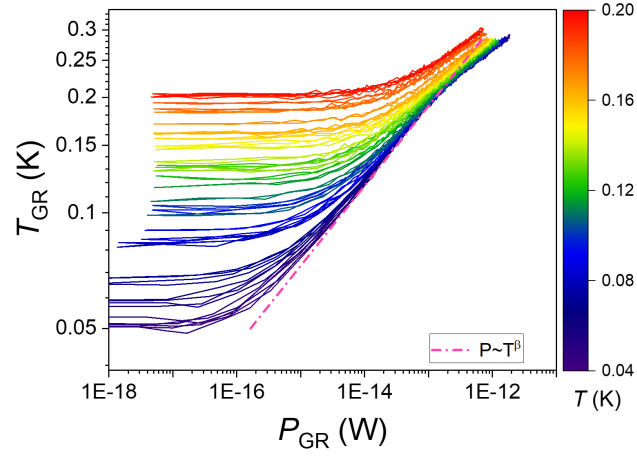


Fig. S6. Graphene temperature T_{GR} versus heating power P_{GR} for different fridge temperatures T .

As $P_{GR} \rightarrow 0$ the plots saturate at corresponding T . For temperatures in the range $T < T_{GR} < \sim 200$ mK the plots reveal $P_{GR} \sim T_{GR}^5$ dependence, above $T_{GR} \sim 200$ mK there seem to be a crossover to a different slope. We speculate that the 200 mK temperature corresponds to onset of heat conductance through quasiparticles in Al electrodes.

S7. Graphene temperature saturation at low fridge temperatures.

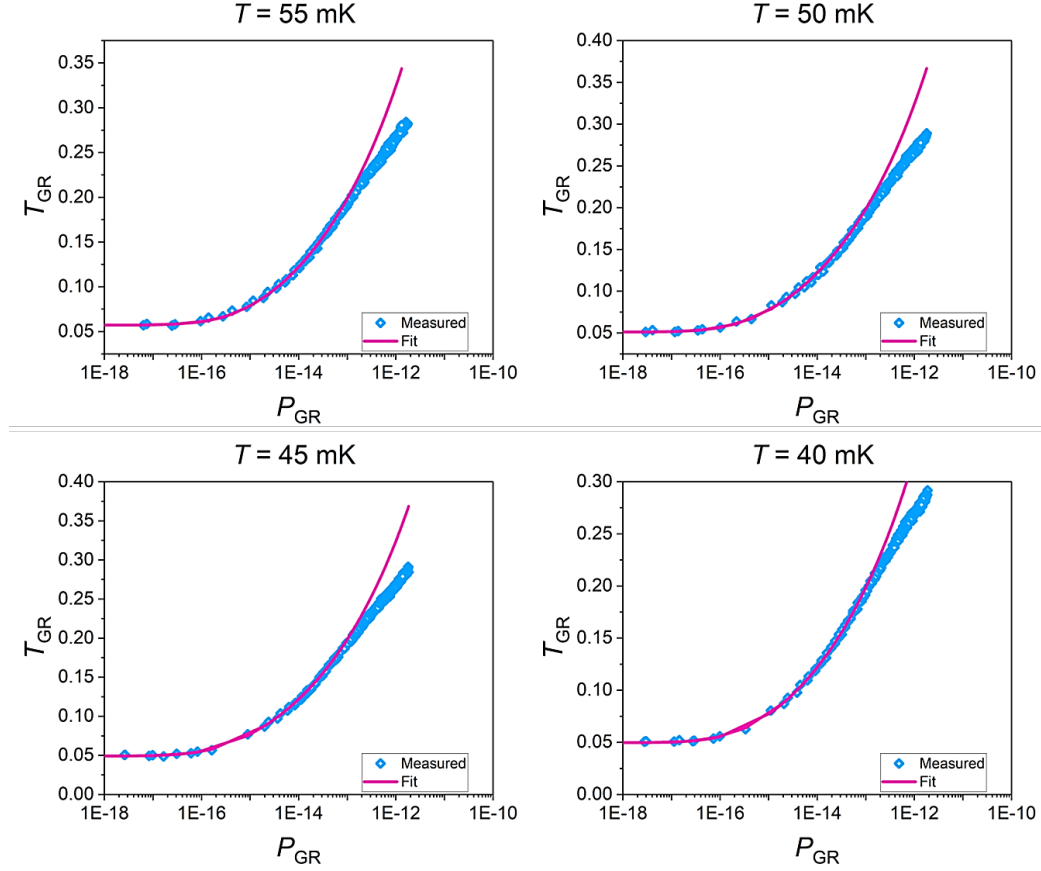


Fig. S7. Experimental data for T_{GR} vs. P_{GR} (rhombs) for fridge temperatures $T = 55, 50, 45, 40$ mK. Solid lines are fits to $T_{GR} = \left(\frac{P_{GR}}{A} + T_0^5 \right)^{1/5}$ with the same parameters $A = 3.5 \cdot 10^{-10}$ W for all plots. Saturation temperatures $T_0 = \lim_{P_{GR} \rightarrow 0} T_{GR}$ extracted from the fits are 57, 51, 49 and 49.5 mK.

S8. Effect of the microwave measurement power: upper bound estimation.

The proper thermalisation of microwave lines is ensured by a set of attenuators on the input channel and a double-junction isolator (34 dB) at the output. All presented measurements were done with VNA instrument power -60 dBm; with 46 dB provided by attenuators and accounting for an extra 7 dB loss in combiner (3 dB) and cables (4 dB), we arrive at the excitation power on a tank circuit -113 dBm. At 50 mK the tank circuit is essentially in a critically coupled regime: the S21 resonance is 7.5 dB deep (*cf* Fig. 1b). For a critically coupled resonator the power P_{diss} dissipated in the resonator is half of the excitation power, i.e -116 dBm (2.5 fW). However, only a small fraction of this power $\alpha = R_Q/R_{GR}$ is adsorbed by graphene, where R_{GR} is the graphene resistance (7.63 M Ω at 50 mK) and $R_Q = Q_i \cdot \sqrt{L/C}$ is the equivalent dissipative resistance of the resonance circuit. Given the tank circuit parameters $Q_i = 440$ (for critically coupled resonator $Q_i = 2f/\Delta f$ and the linewidth Δf is shown in Fig.1b), $L = 47$ nH, $C=1$ pF (by design), we arrive at $R_Q = 95$ k Ω , and $\alpha = 0.012$. The heat conductance $G_{th} = 1.45 \cdot 10^{-14}$ W/K is known from Fig. 3a, so we can estimate the overheating due to the measurement power as $\Delta T_{GR} = \frac{\alpha P_{diss}}{G_{th}} = 1.5$ mK at fridge temperature 50 mK. Reiterating these calculations for all the relevant temperatures, we can compose a plot for ΔT_{GR} at different fridge temperatures:

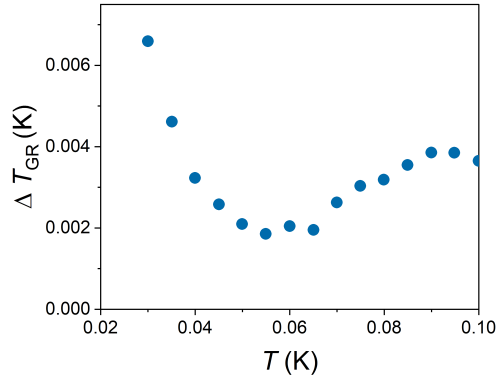


Fig. S8. Upper bound estimation for the graphene overheating due to the microwave measurement power for different fridge temperatures T .

We see that at, say, 40 mK, the overheating due to the measurement power shall not exceed 2.5 mK and therefore could not account for the observed graphene temperature saturation to 50 mK.